

~~***In situ* interactive characteristics of reactive minerals in soil colloids and soil carbon preservation differentially revealed by nanoscale secondary ion mass spectrometry and X-ray absorption fine structure spectroscopy**~~

New strategies for submicron characterization the carbon binding of reactive minerals in long-term contrasting fertilized soils: Implications for soil carbon storage

Jian Xiao¹, Xinhua He², Ying Zhou³, Lirong Zheng⁴, Jialong Hao⁵, Wei Ran¹, Qirong Shen¹, Guanghui Yu^{1,6*}

¹ National Engineering Research Center for Organic-based Fertilizers, Jiangsu Collaborative Innovation Center for Solid Organic Waste Resource Utilization, Jiangsu Provincial Key Lab for Organic Solid Waste Utilization, Nanjing Agricultural University, Nanjing 210095, China

² School of Plant Biology, University of Western Australia, Crawley, WA 6009, Australia

³ Shanghai Institute of Measurement and Testing Technology, Shanghai 201203, China

⁴ Beijing Synchrotron Radiation Facility, Institute of High Energy Physics, Chinese Academy of Sciences, Beijing 100049, China

⁵ Key Laboratory of Earth and Planetary Physics, Institute of Geology and Geophysics, Chinese Academy of Science, Beijing 100029, China

⁶ Department of Plant Pathology, North Carolina State University, Raleigh, NC 27695, USA.

* Correspondence to: G. H. Yu (yuguanghui@njau.edu.cn or gyu6@ncsu.edu)

20 **Abstract.** Mineral binding is a major mechanism for soil carbon (C) stabilization. However, the
submicron information about the *in situ* mechanisms of different fertilization practices affecting
organo-mineral complexes and associated C preservation remains unclear. Here, we applied nano-scale
secondary ion mass spectrometry (NanoSIMS), X-ray photoelectron spectroscopy (XPS), and X-ray
absorption fine structure spectroscopy (XAFS) to examine differentiating effects of inorganic versus
25 organic fertilization on interactions between highly reactive minerals and soil C preservation. To
examine such interactions, soils and their extracted colloids were collected during a 24-year long-term
fertilization period (1990-2014) (no-fertilization, Control; chemical nitrogen (N), phosphorus (P) and
potassium (K) fertilization, NPK; and NPK plus swine manure fertilization, NPKM). The results for
different fertilization conditions showed a ranked soil organic matter (SOM) concentration with
30 NPKM > NPK > Control. Meanwhile, oxalate extracted Al (Al_o), Fe (Fe_o), short range ordered (SRO)
Al (Al_{xps}), Fe (Fe_{xps}), and dissolved organic carbon (DOC) ranked with NPKM > Control > NPK, but
ratios of DOC/Al_{xps} and DOC/Fe_{xps} ranked with NPKM > NPK > Control. Compared with the NPK
treatment, NPKM treatment enhanced the C binding loadings of Al and Fe minerals in soil colloids at
the submicron scale. Furthermore, a greater concentration of highly reactive Al and Fe minerals was
35 present under NPKM than under NPK. Together, these submicron scale findings suggest that both
reactive mineral species and their associations with C are differentially affected by inorganic and
organic fertilization.

Key words: Al and Fe minerals; inorganic and organic fertilization; organo-mineral complexes; reactive
minerals; carbon binding capability; X-ray photoelectron spectroscopy (XPS)

40 1. Introduction

Associations of organic matter (OM) with pedogenic minerals, which are termed as organo-mineral complexes, are known to be key controls in the biogeochemical processes that retain OM in natural soil system (Torn et al., 1997; Kögel-knbaner et al., 2008; Mikutta et al., 2009; Schmidt et al., 2011). Soil OM (SOM) preferentially binds to rough surfaces, which provide a multitude of reactive mineral
45 | surfaces (~~Kögel-Knabner et al., 2008~~; Chen et al., 2014; Vogel et al., 2014). These reactive minerals are also termed as short-range ordered (SRO) meta-stable colloidal minerals in volcanic ejecta (Torn et al., 1997), and serve as the nuclei for soil organic carbon (SOC) storage (Hochella et al., 2008; Kögel-Knabner et al., 2008; Remusat et al., 2012; Vogel et al., 2014). Therefore, reactive Al and Fe minerals in soil play a critical role in determining C stability (Solomon et al., 2012; Hernes et al., 2013).

50 On the other hand, the reactive mineral surface of organo-mineral complexes in the complex soil matrix (mainly the top-soil layer) could be greatly improved through organic amendments to soil, such as the anthropogenic importation of organic fertilizers under long-term experimentation (Schmidt et al., 2011; Hernandez et al., 2012; Yu et al., 2012; Wen et al., 2014a; Abdala et al., 2015). Based on a meta-analysis of 49 sites and 130 observations in the world, Maillard and Angers (2014) found that cumulative manure input had a dominant effect on SOC stock changes when compared to no fertilization and chemical fertilization (Maillard and Angers, 2014). Furthermore, it was estimated that cumulative manure-C input resulted in a relative SOC change factor of 1.26 ± 0.14 (95% CI). Another meta-analysis assessed and identified the effects of improved farming practices on SOC sequestration in China by compiling a data set of 83 studies (Zhao et al., 2015), indicating that SOC concentration and

55

60 stocks at 0-30 cm depth significantly increased when compared to no fertilization and chemical
fertilization. Although our previous results had shown that manure amendments enhanced reactive
components of minerals (i.e., ferrihydrite and allophane) in soils by selective extraction methods,
spectroscopies and high resolution-transmission electron microscopy (HRTEM) observation (Yu et al.,
2012; Wen et al., 2014a and 2014b; Huang et al., 2016) However, little is known about the impacts
65 effects of different fertilization practices on the *in situ* associations between reactive minerals and SOC
in soil colloids at a-submicron scale. ~~Meanwhile, there is few evidence demonstrating that the *in situ*~~
~~preservation capacity of reactive minerals on SOC.~~

In general, *in situ* investigations of natural organo-mineral complexes are restricted to bulk analyses
of operationally defined physical fractions (Hatton et al., 2012 and 2015; Remusat et al., 2012; Vogel et
70 al., 2014). In contrast, techniques for direct visualization at the submicron scale could greatly aid in
gaining a better understanding of the interactions between organic structures and reactive minerals
(Remusat et al., 2012; Vogel et al., 2014; Xiao et al., 2015). For instance, nano-scale secondary ion
mass spectrometry (NanoSIMS) has the potential to examine the spatial integrity of soil
microenvironments and has been designed for high lateral resolution (down to 50 nm) imaging, while
75 still maintaining high mass resolution and high sensitivity (mg kg⁻¹ range) (Herrmann et al., 2007; Xiao
et al., 2015). Previous studies have shown that NanoSIMS is an effective technique for studying natural
organo-mineral complexes at the submicron scale (Herrmann, 2007; Mueller et al., 2012; Remusat et al.,
2012; Hatton et al., 2012 and 2015; Vogel et al., 2014). However, NanoSIMS can not determine the
morphology, elemental composition and mineral species. High-resolution transmission electron

80 microscopy (HRTEM) combined with selected area electron diffraction (SAED) is also a promising
technique that can determine the morphology and provide detailed information on organo-mineral
surfaces, as well as changes in their surface chemistries (Wen et al., 2014a; Yaron-Marcovich et al.,
2005). Although direct observations of organo-mineral complexes by NanoSIMS and HRTEM have
been previously described (Ramos et al., 2013; Vogel et al., 2014; Rumpel et al., 2015), few studies
85 have reported the effects of fertilization practices on the organo-mineral complexes in soil colloids. In
addition, X-ray photoelectron spectroscopy (XPS) can identify the oxidation state of elements on the
surface (2~10 nm) of minerals (Zhu et al., 2014). Compared with XPS technique, X-ray absorption fine
structure spectroscopy (XAFS) is a powerful tool for both identification and quantification of different
mineral phases present in soil colloids (Li et al., 2015; Xiao et al., 2015).

90 Using soil colloids extracted from 24-year fertilized soils (1990-2014), the objectives of this study
were to address 1) the effects of fertilization practices on the quantity and composition of Al and Fe
minerals, and 2) the *in-situ* interactions between SOC and minerals at the submicron scale.

2. Materials and methods

2.1. Soil samples

95 Samples of soil (Ferralic Cambisol, FAO soil taxonomic classification) were from a long-term
(1990-2014) fertilization site in Qiyang, Hunan, Southern China (26°45'N, 111°52'E, 120 m above sea
level). The long-term fertilization experiment, which belongs to the Institute of Agricultural Resources
and Regional Planning, Chinese Academy of Agricultural Sciences, has been under an annual rotation
of wheat and corn cropping system since September 1990. The topsoil contained 61.4% clay, 34.9% silt

100 and 3.7% sand. Three fertilization treatments with 2 replicates or plots (20 m × 10 m) for each treatment were examined as follows: 1) no fertilization (Control), 2) chemical nitrogen (N), phosphorus (P) and potassium (K) (NPK) and 3) a combination of the chemical fertilizers with swine manure (NPKM) (see Fig. S1 for detailed fertilization rates). The NPK and MNPK had the same total application of 300 kg N ha⁻¹ yr⁻¹. The applied N was 100% urea in the NPK, but was 30% from urea with the remaining 70%
105 from swine manure in the MNPK. A 1.0-m-deep cement buffer zone was constructed between each plot. Each soil sample was a composite of twenty random cores (5 cm internal diameter auger) collected at 0-20 cm depth from one replicate plot. The fresh soil was mixed thoroughly, air-dried, and sieved (5 mm) for further analyses.

2.2. Soil colloids extraction and quantitation of highly reactive Al and Fe minerals

110 The soil colloids extraction was based on a previously described method (Schumacher et al., 2005). Briefly, 100 g of fresh soils was suspended in 500 mL of deionized water on a horizontal shaker (170 rpm) for 8 hr at 25 ± 1°C, and centrifuged at 2500 g for 6 min (Fig. S1). Aliquots of the supernatant suspensions and freeze-dried soil colloid samples were then generated. Quantitation of highly reactive minerals, including Al and Fe minerals (Al_o, Fe_o), was performed using the acid ammonium-oxalate
115 extraction method (Kramer et al., 2012). In brief, soil was extracted using 0.275 M ammonium oxalate at pH 3.25 with a 1:100 soil:extractant (w/v) ratio. Ammonium oxalate was used to selectively remove short-range ordered hydrous oxides of Fe and Al such as ~~allophane and ferrihydrite~~ ferrihydrite and allophane.

2.3. HRTEM analysis

120 HRTEM samples were prepared by dropping soil mobile colloids onto carbon coated copper grids. The images were recorded at an acceleration voltage of 200 keV using a JEOL JEM-2100F microscope (JEOL JEM-2100F, Japan), which was at the Analysis and Testing Centre of Nanjing Normal University, China. HRTEM images, selected area electron diffraction (SAED) and energy dispersive X-ray analysis (EDX) were conducted using the JEOL JEM-2100F microscope to characterize soil
125 colloid samples.

2.4. NanoSIMS analyses

For NanoSIMS measurements, several aliquots of the colloidal suspension from these three different fertilization treatments were separately dropped onto a silicon wafer and air-dried. In this study, we chose 6 spots from the NanoSIMS images to show the replicates of each soil colloid sample because
130 the majority of particulate organo-mineral complexes were included and similar according to the characterization of natural colloids (Philippe and Schaumann, 2014; Xiao et al., 2015). For every sample, all 6 spots were analyzed to obtain a reliable data basis for the calculation of the fate of $^{12}\text{C}^-$, $^{27}\text{Al}^{16}\text{O}^-$, and $^{56}\text{Fe}^{16}\text{O}^-$ (Table S2).

The analyses were performed on a NanoSIMS 50L (Cameca, Gennevilliers, France) instrument at
135 the Institute of Geology and Geophysics, Chinese Academy of Sciences, China. Prior to analysis, the gold coating layer (30 nm) and any possible contamination of the sample surface were sputtered using a high primary beam current (pre-sputtering). During the pre-sputtering, the reactive Cs^+ ions were implanted into the sample to enhance the secondary ion yields. The primary beam (~ 0.9 pA) focused at a lateral resolution of 100-200 nm, was scanned over the samples, and the secondary ion images of $^{12}\text{C}^-$,

140 $^{27}\text{Al}^{16}\text{O}^-$, and $^{56}\text{Fe}^{16}\text{O}^-$ were simultaneously collected by electron multipliers with an electronic dead time fixed at 44 ns. The presence of $^{12}\text{C}^-$ ion mass indicated SOC, while the presence of $^{27}\text{Al}^{16}\text{O}^-$ and $^{56}\text{Fe}^{16}\text{O}^-$ demonstrated Al and Fe minerals, respectively. The estimated depth resolution using 16 keV Cs^+ ions as the primary ion beam was about 15 nm. We compensated for the charging due to the non-conductive mineral particles using the electron flood gun of the NanoSIMS instrument. All
145 measurements were conducted in an imaging mode. The dwell time was 1 ms pixel⁻¹ for all acquisitions. Specific details describing NanoSIMS measurements can be found in previous publications (Vogel et al., 2014; Xiao et al., 2015).

The analyses were carried out on different cluster compositions using Image J software with the OpenMIMS plugin (http://www.nrims.hms.harvard.edu/NRIMS_ImageJ.php). In this study, regions of
150 interest (ROIs) were selected according to the intensity of the secondary $^{12}\text{C}^-$ ion mass. Specifically, the visible SOC surface areas were divided into rich and less rich $^{12}\text{C}^-$ ROIs according to the pixel value extracted from the NanoSIMS images. The $^{12}\text{C}^-$ rich ROIs included the areas above 90 pixels and the $^{12}\text{C}^-$ less rich ROIs included the areas in the range of 90-40 pixels under Control and NPK, while the $^{12}\text{C}^-$ rich ROIs were above 50 pixels and the $^{12}\text{C}^-$ less rich ROIs were in the range of 50-30 pixels under
155 NPKM. The threshold option of the Image J software was used to automatically generate the ROIs from these NanoSIMS images. In doing so, the triangle algorithm was used (Vogel et al., 2014; Xiao et al., 2015). The ROIs of the $^{27}\text{Al}^{16}\text{O}^-$ and $^{56}\text{Fe}^{16}\text{O}^-$ images were combined afterwards to obtain the ROIs according to the distribution of the $^{12}\text{C}^-$ rich ROIs and $^{12}\text{C}^-$ less rich ROIs under different fertilizations conditions (Table S2).

160 **2.5. XPS analyses**

The sample preparation for the XPS procedures was adapted from Gerin et al. (2003). The XPS data were collected using a PHI 5000 Versa Probe X-ray photoelectron spectrometer (UIVAC-PHI, Japan) equipped with a monochromatized Al K α X-ray source (1486.69 eV). The binding energy scale was corrected using the adventitious hydrocarbon C 1s spectrum (C 1s = 284.6 eV) (Zhu et al., 2014).
165 The analyzed zone corresponded to a 300 μm \times 300 μm elliptical spot. The surface charge induced by the photo ejection process was balanced using a flood gun at 6 eV. To optimize the signal to noise ratio, spectra were recorded at a detector resolution corresponding to 0.125 eV per channel. The base pressure in the spectrometer was 6.7×10^{-10} Torr. The XPS data analyses were performed using XPSPEAK 4.1 with Shirley background correction, as referenced at <http://www.lasurface.com/xps/index> and
170 <http://srdata.nist.gov/xps/Default.aspx>. No fixed full width at half maximum (FWHM) values were determined for the spectra of soil colloids collected under contrasting fertilization treatments. Gaussian-Lorentzian ratios were freely fit for all peaks in this study (Liang et al., 2008).

2.6. XAFS spectra analyses

Fe K-edge X-ray absorption fine structure (XANES) and extended X-ray absorption fine structure
175 (EXAFS) spectra were recorded at the beamline 1W1B at the XAFS Station of the Beijing Synchrotron Radiation Facility (BSRF, Beijing, China) using a Si (111) double-crystal monochromator. The storage ring was operated at 2.5 GeV with the electron current decreasing from 240 to 160 mA within approximately 8 hrs. Samples were ground into fine powders and brushed onto tapes, which were then stacked together to yield approximately one X-ray-absorption length at their corresponding metal edges.

180 The intensities of incident and transmitted X-rays were monitored by ionization chambers filled with nitrogen gas. All reported spectra were measured at 20°C. Spectra were collected in quick-scan and transmission mode. XANES spectra were recorded with 0.5 eV step, counting 10 s from 7,100 to 7,800 eV. EXAFS spectra were recorded up to $k = 14.0 \text{ \AA}^{-1}$, using 1 eV steps and counting for 100–200 s per scan. To improve data quality, 5 XANES scans and 5 EXAFS scans were recorded for each sample. The

185 X-ray energy scale was calibrated to the iron K-edge (7112.0 eV) using an iron metal foil prior to XAFS acquisition. Averaged spectra were normalized using Athena (Version 2.1.1, California, USA) software, and EXAFS data were extracted using the Autoback routine, using the same program. The spectra were normalized by subtracting a first-order polynomial fitted to the data from –100 to –30 eV before the edge and subsequently dividing through a second-order polynomial fitted to the data from 60 to 450 eV

190 above the edge. –Linear combination fitting (LCF) of XANES data were performed with the respective functions of Athena. EXAFS spectra were extracted using the Autobk algorithm (Rbkg = 0.9; k-weight = 3, spline k-range 0–11.8 \AA^{-1}). The Fe K-edge XANES spectra with LCF of eight standard iron samples were used to precisely characterize the composition of Fe minerals (Baumgartner et al., 2013; Senn et al., 2015). The standard iron samples of ferrous sulfate, ferrous oxalate, ferric sulfate, ferric oxalate,

195 goethite, hematite, ferrihydrite, and maghemite were also recorded in transmission mode, which were purchased or synthesized (Table S3). A standard was considered to have a substantial contribution if it accounted for more than 10% of a linear combination fit. The quality of the LCF was given by the residual value, the goodness-of-fit parameter R , defined by $R = 6[I_{\text{exp}}(E) - I_{\text{cal}}(E)]^2 / 6[I_{\text{exp}}(E)]^2 \times 100$ where I_{exp} and I_{cal} are the absorption of the experimental and calculated spectra, respectively.

200 2.7. Chemical analyses

The concentration of SOC was quantified using a CN analyzer (Vario EL, Elementar GmbH, Hanau, Germany), while SOM was $1.724 \times \text{SOC}$. Soil pH was determined using a pH electrode at a 1:5 soil: distilled water ratio. The concentration of Fe and Al was quantified by inductively coupled plasma atomic emission spectroscopy (710/715 ICP-AES, Agilent, Australia). The concentration of DOC was
205 determined by a TOC/TN analyzer (multi N/C 3000, Analytik Jena AG, Germany).

2.8. Statistical analyses

One-way analysis of variance (ANOVA) was used to test the effects of long-term fertilization on reactive iron minerals in the soil. Significant differences between treatments (means \pm SE, $n = 3$) were determined by Tukey's HSD post hoc test at $P < 0.05$, where the conditions of normality and
210 homogeneity of variance were met.

3. Results

3.1. Concentration and morphology of organo-mineral complexes in soil colloids under contrasting fertilizations

Compared with a soil pH of 5.47 under Control, the soil pH significantly decreased to 4.15 under
215 NPK but significantly increased to 5.84 under NPKM (Table 1). SOM concentrations in different fertilization treatments ranked as $\text{NPKM} > \text{NPK} > \text{Control}$ (Table 1). Oxalate extracted Al (Al_o), Fe (Fe_o), SRO Al (Al_{xps}), Fe (Fe_{xps}), and DOC ranked as $\text{NPKM} > \text{Control} > \text{NPK}$, but ratios of $\text{DOC}/\text{Al}_{\text{xps}}$ and $\text{DOC}/\text{Fe}_{\text{xps}}$ ranked as $\text{NPKM} > \text{NPK} > \text{Control}$ (Table 1).

To get insight into the spatial distribution of SOM associated with reactive mineral particles, we

220 used both HRTEM and NanoSIMS to acquire *in situ* observations of such associations. At the nanometer scale, the HRTEM images of extracted soil colloids provided direct visualization of the presence of soil SRO minerals from Control-, NPK- and NPKM-fertilized samples (Fig. 1). Soil minerals showed amorphous and crystalline patterning in different regions (Fig. 1-a, b). The SAED (selected area electron diffraction) pattern further demonstrated that the amorphous mineral species were dominated by Al, Si, and O, while the crystalline minerals were mainly composed of Fe and O (Fig. 1-c, d).

225 —The NanoSIMS images of $^{12}\text{C}^-$, $^{27}\text{Al}^{16}\text{O}^-$, and $^{56}\text{Fe}^{16}\text{O}^-$ ion masses showed the submicron elemental distribution and spatial heterogeneity in the soil colloids (Fig. 2). The color bar from blue to white showed that the concentration of $^{12}\text{C}^-$, $^{27}\text{Al}^{16}\text{O}^-$, and $^{56}\text{Fe}^{16}\text{O}^-$ ion masses was from weak to strong on each image. Under different fertilizations, organo-mineral complexes also distributed in a heterogeneous way as indicated by the color bar on the NanoSIMS images (from blue to white) at the submicron scale (Figs. 2 and S2).

3.2. Binding capability of C by Al and Fe minerals

235 We next used the region of interests (ROIs) to explore the C binding capability of Al and Fe minerals. Fig. S2 was presents a representative NanoSIMS image showing the position of region of interests (ROIs) among the several replicates (spots) of different fertilization treatments (Control: 8 replicates; NPK: 6 replicates; NPKM: 6 replicates, respectively). Based on the pixel value of secondary $^{12}\text{C}^-$ ion mass in all spots from different each fertilization treatments sample, the selected ROIs were identified. The selected ROIs were further divided into $^{12}\text{C}^-$ rich- and $^{12}\text{C}^-$ less rich- ROIs (Fig. S2-and

240 ~~Table S2).~~ Table S2 lists the quantification of $^{12}\text{C}^-$ rich ($^{12}\text{C}^-$ -R) and $^{12}\text{C}^-$ less-rich ($^{12}\text{C}^-$ -LR) ROIs. The
 area percentage of the $^{12}\text{C}^-$ rich- or $^{12}\text{C}^-$ less rich- ROIs accounted for 7.47% or 40.18 %, 10.80% or
 27.64 % and 8.23% or 37.99% under Control, NPK and NPKM, respectively (Table S2). The area of
 245 percentage for the Control and the NPKM was similar but different from the NPK, suggesting that
compared to no fertilization, chemical fertilizer can change organo-mineral associations at the
submicron scale in soil colloids, but chemical plus organic fertilization can eliminate the effect of
chemical fertilizaiton on organo-mineral associations. Interestingly, the box plots (Fig. 3) of
 $^{12}\text{C}^-/^{27}\text{Al}^{16}\text{O}^-$ (a, b) and $^{12}\text{C}^-/^{56}\text{Fe}^{16}\text{O}^-$ (c, d) ratios showed that both the median and the mean value were
 higher under NPKM than those under NPK. These results provided *in-situ* observation evidence at the
submicron scale demonstrating that more organic C had been bound by Al and Fe minerals under
 250 NPKM than under NPK (Figs. 2 and 3), which is consistent with previous results from bulk analysis
(Maillard and Angers, 2014). ~~These results suggest that more organic C may be bound by Al and Fe~~
~~minerals under NPKM than under NPK (Figs. 2 and 3).~~

3.3. Chemical speciation of reactive minerals and C

The XPS Al $2p_{3/2}$ peak-fitting results (Table 2 and Fig. 4) showed that 45% allophane (~73.80 eV),
 255 29.4% of boehmite (~74.5 eV) and 26% Al Ox (~75.40 eV) were **present** in soil colloids under NPKM.
 In contrast, approximately 43% and 34% of allophane were observed in soil colloids under NPK and
 Control, respectively. Considering higher (over 5 times) total Al concentrations in soil colloids under
 NPKM than NPK (Table 1), the amount of allophane in soil colloids under NPKM is approximately 5
 times higher than that of NPK.

260 Linear combination fitting (LCF) of soil colloids (Fig. 5 and Table 3) showed that goethite (56.8%-67.0%) and hematite (14.9%-25.0%) were prominent under all three fertilizations. The remaining Fe phases were composed of the less crystalline ferrihydrite species. The percentage of ferrihydrite was the highest under NPKM ($18.0 \pm 0.02\%$), followed by Control ($16.0 \pm 0.03\%$) and NPK ($6.30 \pm 0.02\%$). In view of the better C binding and potential preservation capability of ferrihydrite
265 when compared to goethite and hematite (Baker et al., 2010; Kramer et al., 2012; Lalonde et al., 2012; Xiao et al., 2015), it is reasonable to conclude that there is greater C loading by Fe minerals under organic fertilization than under chemical fertilization. This result is consistent with previous meta-analysis (Maillard and Angers, 2014) but provides *in-situ* observation evidence at the submicron scale.

270 Furthermore, Fe K-edge EXAFS was used for qualitative analysis of the composition of Fe minerals in soil colloids. The Fe k^3 -weighted EXAFS spectra (Fig. 6, left) showed that the spectral features of soils colloids under Control and NPKM were more similar to those of goethite, hematite, and ferrihydrite than to other minerals or compounds, suggesting that those Fe minerals are mainly composed of goethite, hematite, and ferrihydrite. The spectral features of the soils under NPK were
275 more similar to those of goethite and hematite than to those of other minerals or compounds, supporting that those Fe minerals are mainly composed of goethite and hematite rather than short-range ordered ferrihydrite. Specifically, the EXAFS of Fe oxides showed double antinodes at 9.2 and 11.6 \AA^{-1} under Control and NPKM, whereas triple antinodes were observed under NPK at 9.2, 10.3 and 11.6 \AA^{-1} (Fig. 6, left). Double antinodes were found in hematite and ferrihydrite, whereas triple antinodes were

280 observed in goethite. These results implied that the coordination environment for Fe-Fe linkages in Control and NPKM samples might be different from that in NPK samples because the observed peak primarily derived from the Fe-Fe coordination in goethite (Mitsunobu et al., 2012).

Fourier transforms showed that Fe minerals under Control and NPKM had most of the features observed in goethite, hematite, and ferrihydrite [i.e., first peak (Fe-O) and second peak (edge-sharing Fe-Fe)] and amplitude of multiple-scattering peak at 5.2 Å. Specifically, the first shell at 1.5 Å
285 corresponds to the Fe-O coordination, and the intensity and position were approximately identical between the Control or NPKM treated soil colloids and ferrihydrite spectra. In contrast, the second shell identified at $R + \Delta R = 2.3\text{-}3.5$ Å corresponding to the Fe-Fe coordination was smaller than that of ferrihydrite. These results indicated that Fe in the Control and NPKM treated soil colloids might have a
290 weaker Fe-Fe linkage than that in ferrihydrite.

In addition, the XPS C 1s peak-fitting results (Table 2 and Fig. 4) demonstrated that aromatic C (Ar-C-C/Ar-C-H, ~284.6 eV) was dominant under all three fertilizations, with the highest percentage (75.86%) under NPKM, followed by NPK (62.51%) and Control (62.26%). In contrast, percentages of other carbon groups, i.e., ether or alcohol carbon (C-O) and ketone or aldehyde carbon (C=O), were
295 lowest under NPKM among the three contrasting fertilization treatments.

4. Discussion

4.1. Long-term organic fertilization increased the concentration of highly reactive Al and Fe minerals and their soil C binding capacity

Selective extraction method (Table 1) showed that organic fertilization increased 36.36% of highly

300 reactive Al (Al_o) and 33.33% of highly reactive Fe minerals (Fe_o) compared with Control treatment, but increased 63.64% of Al_o and 46.67% of Fe_o compared with NPK treatment. ~~Ultimately it was obvious that~~ Therefore, organic fertilization ~~could has been shown to~~ facilitates the formation of highly reactive Al and Fe minerals. By ^{27}Al nuclear magnetic resonance (NMR) and Fourier- transform infrared spectroscopy (FTIR) spectroscopy, Wen et al. (2014b) confirmed the presence of amorphous Al
305 as allophane and imogolite in soil colloids under no fertilization and organic fertilization but not under chemical fertilization. ~~and the previous studies had also got the similar regular pattern according to quantitative chemical analyses (Yu et al., 2012; Wen et al., 2014a, b; Wu et al., 2014; Huang et al., 2016).~~ However, ~~but~~ the direct potential of C preservation capacity by Al and Fe minerals under different fertilizations regimes remains unexplored. In this study, the ROI analyses of NanoSIMS *in-situ*
310 observation (Fig. 3) provided direct evidence that long-term organic fertilization strengthened the SOC binding and preservation capability of Al and Fe minerals in soil colloids as well as a highly spatial heterogeneity ~~of soil colloids~~ at the submicron scale. Additionally, colloids from the NPKM treated soil had higher ratios of DOC/Al_{xps} and DOC/Fe_{xps} than those under Control and NPK (Table 1), which was compatible with the assumption suggested by the NanoSIMS and HRTEM. These results could be
315 derived from a long-term continuous organic C input that might have enriched soil microbial communities and then in turn supported an efficient formation of the concomitant organo-mineral aggregates (Wild et al., 2014; Basler et al., 2015).

Moreover, it was notable that higher proportion ~~greater amounts~~ of aromatic C (Ar-C-C/Ar-C-H)

while lesslower proportion of ether or alcohol carbon (C-O) or ketonic or aldehyde carbon (C=O) were

observed under NPKM than under NPK or Control, which indicated that additional aromatic functional

groups might have a priority ~~had been attached to~~ to attaching to the highly reactive Al and Fe

minerals compared with other carbon groups. ~~under NPKM~~. This result is also supported by C 1s

near-edge X-ray fine structure (NEXAFS) spectroscopy that compared to the NPK treatment, the

NPKM treatment markedly increased the percentages of both the aromatic (283.0–286.1 eV) and

phenolic (286.2–287.5 eV) groups over 2.8-fold (Huang et al., 2016). Moreover, the XPS C 1s

peak-fitting results (Table 2 and Fig. 4) demonstrated that the highest percentage of aromatic C (75.86%)

was present under NPKM, followed by NPK (62.51%) and Control (62.26%). The previous

investigation had shown that aromatic C in composted dairy manure accounted for approximately 30%

of the total C, taking advantage of solid-state ¹³C nuclear magnetic resonance (NMR) spectroscopy

(Liang et al., 1996). And the addition of manure-based amendments increased SOC and enhanced

aggregate stability (Mikha et al., 2015). But it is unclear whether manure is direct contributed to

aromatic C increase or first utilized by microbes and then contributed to aromatic C increase in this

study. Since aromatic compounds are preferentially retained at the interface of reactive minerals and

that long-term C storage by SRO minerals has occurred via the mechanism of chemical retention with

dissolved aromatic acids (Kramer et al., 2012; Huang et al., 2016). These results were due to that the

long-term continuous organic C input could improve the spatial arrangement within the mineral matrix

(i.e., more amorphous minerals), the fine-scale redox environment (i.e., appropriate pH), microbial

[ecology \(i.e., appropriate pH, manure\) and interaction with mineral surfaces under fertile and weakly acidic conditions \(Wild et al., 2014; Basler et al., 2015; Lehmann and Kleber, 2015\).](#)

4.2. Long-term organic fertilization modified the composition of highly reactive Al and Fe minerals

Our results from both XPS, ~~and NanoSIMS and~~ Fe K-edge XAFS showed that organic fertilization facilitated the formation of highly reactive Al and Fe minerals, e.g., allophane, imogolite, and ferrihydrite (Tables 2-3 and Figs. 34-6), which could further explain why long-term organic manure fertilization was able to ~~improve~~^{alter} the C and N binding capacity of Al and Fe minerals. The data from the TOC and ICP-AES (Table 1) also supported that soils under NPKM contained significantly higher percentages of Al_o, Fe_o, SRO minerals, and SOM than those under NPK. The results from HRTEM and SAED (Fig. 1) further showed that soil colloids under NPKM were composed of large amounts of meta-stable amorphous or SRO minerals (e.g., allophane, imogolite and ferrihydrite), which could form stable organic-mineral bonds through anion and inner-sphere ligand-exchange reactions and would thus be well-suited to physically protecting geometries (Torn et al., 1997; Yu et al., 2012; Basler et al., 2015).

[It would be an innovative method using the ratio of \$^{12}\text{C}/^{27}\text{Al}^{16}\text{O}^-\$ and \$^{12}\text{C}/^{56}\text{Fe}^{16}\text{O}^-\$ on NanoSIMS images to quantify the stronger binding ability in NPKM treatment compared with the other treatments \(Fig. 3\).](#) These results are consistent with previous studies using ^{27}Al ~~nuclear magnetic resonance (NMR)~~ spectroscopy and ~~Fourier-transform infrared spectroscopy (FTIR)~~ (Yu et al., 2012; Wen et al., 2014a,b; Wu et al., 2014). ~~Using Fe K-edge XANES spectroscopy, Huang et al. (2016) also showed that reactive Fe minerals were mainly composed of less crystalline ferrihydrite in the M-treated soil and more~~

crystalline goethite in the NPK-treated soil. By measuring the composition of manure, Wen et al. (2014b)
had shown that the reactive minerals introduced by the manures were very limited, ruling out the
possibility that fertilizers introduced reactive fractions. Furthermore, Huang et al. (2016) indicated that
organic fertilization increased the iron freeness index (i.e., Fe_d/Fe_t ratio) when compared to no
fertilization and chemical fertilization, suggesting a high degree of soil weathering in organic
fertilization. Therefore, we suggest that organic fertilization treatments in situ enhance reactive minerals
by the transformation of minerals. This is supported by a simulated study from Huang et al. (2016) that
addition of oxalic acid to soil colloids can promote the transformation from Fe(III) to ferrihydrite.
Another previous report also indicated that the low-molecular-weight (LMW) organic acid may
incorporate into the network structure of SRO minerals, inhibiting further growth of SRO minerals (Xu
et al., 2010).~~Furthermore, high amounts of organic acid in NPKM fertilized soils may play a critical role~~
~~in promoting the formation of reactive minerals (Huang et al., 2016).~~

In addition, previous studies have shown that the formation of highly reactive Al and Fe minerals
could greatly benefit the binding and potential preservation of SOC (Torn et al., 1997; Wen et al., 2014a;
Xiao et al., 2015). Especially, reactive Fe minerals may responsible for the retention of aromatic C and
O-alkyl C in soils (Huang et al., 2016). Under favorable conditions, SOC turnover in soil colloids with
highly reactive Al and Fe minerals could persist in tephra beds for at least 250,000 yrs (Parfitt, 2009).
Accumulation of highly reactive Al and Fe minerals in soil colloids could therefore improve SOC
sequestration under long-term organic manure fertilization. Furthermore, soil colloids usually consist of
mixtures or complexes of hydrous oxides of Fe, Al and natural organic matter, which have important

implications for deposition, aggregation, and sorption processes (Schumacher et al., 2005; Herrmann et al., 2007; Mueller et al., 2012).

4.3. Environmental implications and technical challenges

Soils are highly complex materials that are structurally and elementally heterogeneous across a wide range of spatial and temporal scales (Herrmann et al., 2007; Mueller et al., 2012; Vogel et al., 2014). In porous media the stability, transport, and deposition of colloids, which usually consist of mixtures or complexes of hydrous oxides of Fe, Al, and natural organic matter, are strongly affected by the mobilized colloidal particles and specific surface area (Kaiser and Guggenberger, 2003; Schumacher et al., 2005). By combining HRTEM, NanoSIMS, XPS and/or XANES technique, the present study investigated the previously unknown highly reactive mineral elements and their spatial distribution patterns under contrasting fertilizations. This strategy has the following key advantages: HRTEM, NanoSIMS images and elemental mapping with sufficient resolution are able to illustrate the specific relationship and spatial heterogeneity of organic, highly reactive mineral complexes under contrasting fertilizations, while decomposition of XPS and Fe K-edge XANES peaks to definite semi-quantitative determinations shows the elemental valence states and compositions. Nevertheless, we are still faced with the challenge of how to utilize spatial information to parameterize models for handling the complex, stochastic interactions between organo-mineral complexes and their microenvironments, including a range of biogeochemical transformation influenced by different fertilization treatments at the submicron scale (Remusat et al., 2012; Abdala et al., 2015; Hatton et al., 2015). **Because of the highly heterogeneous distribution of mineral elements/C-functional groups in soils, investigation on**

more regions in more samples is necessary to obtain solid relationships between organic C and mineral elements using the NanoSIMS *in situ* observation. Meanwhile, inadequate sample preparation to avoid artefacts is also a challenge, which may introduce a bias in the interpretation of NanoSIMS data and location of regions-of-interest (Herrmann et al., 2007). In addition, the complexity of iron chemistry in soils also makes Fe XANES and EXAFS characterization a challenge. For example, the accuracy of the LCF results is strongly affected by the correctness of the applied set of predictor variables (Prietz et al., 2007). And EXAFS only provides average structural information over a short-range order, therefore it fails to determine if the minerals are crystalline or amorphous (Li et al., 2015), which is important in understanding the stabilization of organic carbon. With the enough soil samples and the improvement of sample preparation, these limitations can be well overcome, and the strategy is expected to receive wide applications in the fields of environmental science.

5. Conclusions

In this study, we showed that long-term (1990-2014) organic fertilization increased the carbon binding loading and the potential preservation capacity of soil colloids at the submicron scale. ~~through the formation of highly reactive Al and Fe minerals. Meanwhile, the organo-mineral complexes in the colloids extracted from fertilized soils showed the highly spatial heterogeneity at the submicron scale. These submicron scale findings suggest that both reactive mineral species and their associations with C~~ are differentially affected by inorganic and organic fertilization. ~~The quantities of highly reactive Al minerals (allophane, imogolite) and highly reactive Fe minerals (ferrihydrite) were significantly higher under NPKM than under Control and NPK. Our results~~ This may be attributed to a greater concentration

of highly reactive Al and Fe minerals present under NPKM than under NPK. Meanwhile, we also demonstrated that the combination of nano-scale secondary ion mass spectrometry (NanoSIMS) ~~and~~, high resolution-transmission electron microscopy (HRTEM), X-ray absorption fine structure spectroscopy (XAFS), and X-ray photoelectron spectroscopy (XPS). is a promising ~~strategy-approach~~ to distinguish relationships between C preservation and minerals in natural soil colloids as well as the potential for SOM accumulation under inorganic and organic fertilizations at the submicron scale. The strategy paves the way toward in situ characterization of organo-mineral associations, which is critical in understanding their associated SOM accumulation and soil carbon storage.

Supplementary material related to this article is available online at:
<http://www.biogeosciences.net/>

Acknowledgment. The authors thank B.R. Wang for his assistance in soil sampling in the Qiyang Long-term Fertilization Station. This work was jointly financially supported by National Natural Science Foundation of China (41371248 and 41371299), Natural Science Foundation of Jiangsu Province of China (BK20131321), the Qing Lan Project, the Innovative Research Team Development Plan of the Ministry of China (IRT1256), the 111 Project (B12009), the Priority Academic Program Development (PAPD) of Jiangsu Higher Education Institutions, and Research Project of Shanghai Municipal Bureau of Quality and Technical Supervision (I00RJ1414).

References

Abdala, D.B., da Silva, I.R., Vergutz, L., and Sparks, D.L.: Long-term manure application effects on

phosphorus speciation, kinetics and distribution in highly weathered agricultural soils, *Chemosphere*, 119, 504-514, 2015.

440 Baker, L.L., Strawn, D.G., Vaughan, K.L., and McDaniel, P.A.: XAS study of Fe mineralogy in a chronosequence of soil clays formed in basaltic cinders, *Clays Clay Min.*, 58, 772-782, 2010.

Basler, A., Dippold, M., Helfrich, M., and Dyckmans J.: Microbial carbon recycling-an underestimated process controlling soil carbon dynamics-Part 1: A long-term laboratory incubation experiment, *Biogeosciences*, 12, 5929-5940, 2015.

445 Baumgartner, J., Morin, G., Menguy, N., Perez Gonzalez, T., Widdrat, M., Cosmidis, J., and Faivre, D.: Magnetotactic bacteria form magnetite from a phosphate-rich ferric hydroxide via nanometric ferric (oxyhydr)oxide intermediates, *Proc. Natl. Acad. Sci.*, 110, 14883-14888, 2013. Chen, C.M., Dynes, J.J., Wang, J., Karunakaran, C., Sparks, D.L.: Soft X-ray spectromicroscopy study of mineral-organic matter associations in Pasture soil clay fractions, *Environ. Sci. Technol.*, 48, 6678-6686, 2014.

Childs, C.W., Inoue, K., Seyama, H., Soma, M., Theng, B.K.G., and Yuan, G.: X-ray photoelectron spectroscopic characterization of Silica Springs allophane, *Clay Min.*, 32, 565-572, 1997.

Crist, B.V.: Handbook of monochromatic XPS spectra, XPS International, LLC, Mountain View, USA, 2000.

455 Gerin, P., Genet, M., Herbillon, A., Delvaux, B.: Surface analysis of soil material by X-ray photoelectron spectroscopy, *Eur. J. Soil Sci.*, 54, 589-604, 2003.

Hatton. P.J., Remusat, L., Zeller, B., Derrien, D. A multi-scale approach to determine accurate

elemental and isotopic ratios by nano-scale secondary ion mass spectrometry imaging, *Rap. Commu. Mass Spectro.*, 26, 1363-1371, 2012.

460 Hatton. P.J., Castanha, C., Torn, M.S., and Bird, J.A.: Litter type control on soil C and N stabilization dynamics in a temperate forest, *Glob. Chang. Biol.*, 21, 1358-1367, 2015.

Hernandez, Z., Almendros, G., Carral, P., Alvarez, A., Knicker, H., Perez-Trujillo, J.P.: Influence of non-crystalline minerals in the total amount, resilience and molecular composition of the organic matter in volcanic ash soils (Tenerife Island, Spain), *Eur. J. Soil Sci.*, 63, 603-615, 2012.

465 Hernes, P.J., Kaiser, K., Dyda, R.Y., Cerli, C.: Molecular trickery in soil organic matter: hidden lignin, *Environ. Sci. Technol.*, 47, 9077-9085, 2013.

Herrmann, A.M., Ritz, K., Nunan, N., Clode, P.L., Pett-Ridge, J., Kilburn, M.R., Murphy, D.V., O'Donnell, A.G., Stockdale, E.A.: Nano-scale secondary ion mass spectrometry-A new analytical tool in biogeochemistry and soil ecology: A review article, *Soil Biol. Biochem.*, 39, 1835-1850,
470 2007.

Hochella, M.F.Jr., Lower, S.K., Maurice, P.A., Penn, R.L., Sahai, N., Sparks, D.L., and Twining, B.S.: Nanominerals, mineral nanoparticles, and Earth systems, *Science*, 319, 1631-1635, 2008.

Huang, C.C., Liu, S., Li, R.Z., Sun, F.S., Zhou, Y., and Yu, G.H.: Spectroscopic evidence of the improvement of reactive iron mineral content in red soil by long-term application of swine manure,
475 PLoS One, 11, e0146364, 2016.

Kaiser, K., and Guggenberger, G.: Mineral surfaces and soil organic matter, *Eur. J. Soil Sci.*, 54, 219-236, 2003.

- Kögel-Knabner, I., Guggenberger, G., Kleber, M., Kandeler, E., Kalbitz, K., Scheu, S., Eusterhues, K., and Leinweber, P.: Organo-mineral associations in temperate soils: Integrating biology, mineralogy, and organic matter chemistry, *J. Plant Nutr. Soil Sci.*, 171, 61-82, 2008.
- Kramer, M.G., Sanderman, J., Chadwick, O.A., Chorover, J., Vitousek, P.M.: Long-term carbon storage through retention of dissolved aromatic acids by reactive particles in soil, *Glob. Chang. Biol.*, 18, 2594-2605, 2012.
- Lalonde, K., Mucci, A., Ouellet, A., Gelinas, Y.: Preservation of organic matter in sediments promoted by iron, *Nature*, 483, 198-200, 2012.
- [Lehmann, J., and Kleber M.: The contentious nature of soil organic matter, *Nature*, 528, 60-68, 2015.](#)
- Li, W., Joshi, S.R., Hou, G.J., Burdige, D.J., Sparks, D.L., and Jaisi, D.P.: Characterizing phosphorus speciation of Chesapeake Bay sediments using chemical extraction, ^{31}P NMR, and X-ray absorption fine structure spectroscopy, *Environ. Sci. Technol.*, 49, 203-211, 2015.
- Liang, B., Lehmann, J., Solomon, D., Sohi, S., Thies, J.E., Skjemstad, J.O., Luizao, F.J., Engelhard, M.H., Neves, E.G., and Wirick, S.: Stability of biomass-derived black carbon in soils, *Geochim. Cosmochim. Acta*, 72, 6069-6078, 2008.
- [Liang, B.C., Gregorich, E.G., Schnitzer M., and Voroney R.P.: Carbon mineralization in soils of different textures as affected by water-soluble organic carbon extracted from composted dairy manure, *Biol. Fertil. Soils*, 21, 10-16, 1996.](#)
- [Maillard, E., and Angers, D. A.: Animal manure application and soil organic carbon stocks: a meta-analysis, *Glob. Chang. Biol.*, 2, 666-679, 2014.](#)

500

Mikha, M. M., Hergert, G. W., Benjamin, J. G., Jabro, J. D., and Nielsen, R. A.: Long-term manure impacts on soil aggregates and aggregate-associated carbon and nitrogen, Soil Sci. Soc. Amer. J., 79, 2, 626-636, 2015.

505

Mikutta, R., Schaumann, G.E., Gildemeister, D., Bonneville, S., Kramer, M.G., Chorover, J., Chadwick, O.A., and Guggenberger, G.: Biogeochemistry of mineral-organic associations across a long-term mineralogical soil gradient (0.3-4100kyr), Hawaiian Islands, Geochim. Cosmochim. Acta, 73, 2034-2060, 2009.

510

Mitsunobu, S., Shiraishi, F., Makita, H., Orcutt, B.N., Kikuchi, S., Jorgensen, B.B., Takahashi, Y.: Bacteriogenic Fe(III) (oxyhydr)oxides characterized by synchrotron microprobe coupled with spatially resolved phylogenetic analysis, Environ. Sci. Technol., 46, 3304-3311, 2012.

Mueller, C.W., Kölbl, A., Hoeschen, C., Hillion, F., Heister, K., Herrmann, A.M., and Kögel-Knabner, I.: Submicron scale imaging of soil organic matter dynamics using NanoSIMS-From single particles to intact aggregates, Org. Geochem., 42, 1476-1488, 2012.

Parfitt, R.L.: Allophane and imogolite: role in soil biogeochemical processes, Clay Min., 44, 135-155, 2009.

Philippe, A. and Schaumann, G.E.: Interactions of dissolved organic matter with natural and engineered inorganic colloids: A review, Environ. Sci. Technol., 48, 8946-8962, 2014.

515

Prietzl, J., Thieme, J., Eusterhues, K., and Eichert, D.: Iron speciation in soils and soil aggregates by synchrotron-based X-ray microspectroscopy (XANES, μ -XANES), Europ. J. Soil Sci., 58, 1027-1041, 2007.

- Ramos, M., Ferrer, D., Martinez-Soto, E., Lopez-Lippmann, H., Torres, B., Berhault, G., and Chianelli, R.R.: In-situ HRTEM study of the reactive carbide phase of Co/MoS₂ catalyst, *Ultramicroscopy*, 127, 64-69, 2013.
- Remusat, L., Hatton, P.J., Nico, P.S., Zeller, B., Kleber, M., Derrien, D.: NanoSIMS study of organic matter associated with soil aggregates: advantages, limitations, and combination with STXM, *Environ. Sci. Technol.*, 46, 3943-3949, 2012.
- Rumpel, C., Baumann, K., Remusat, L., Dignac, M.F., Barré, P., Deldicque, D., Glasser, G., Lieberwirth, I., and Chabbi, A.: Nanoscale evidence of contrasted processes for root-derived organic matter stabilization by mineral interactions depending on soil depth, *Soil Biol. Biochem.*, 85, 82-88, 2015.
- Schmidt, M.W.I., Torn, M.S., Abiven, S., Dittmar, T., Guggenberger, G., Janssens, I.A., Kleber, M., Kögel-Knabner, I., Lehmann, J., Manning, D.A.C., Nannipieri, P., Rasse, D.P., Weiner, S., Trumbore, S.E.: Persistence of soil organic matter as an ecosystem property, *Nature*, 478, 49-56, 2011.
- Schumacher, M., Christl, I., Scheinost, A.C., Jacobsen, C., Kretzschmar, R.: Chemical heterogeneity of organic soil colloids investigated by scanning transmission X-ray microscopy and C-1s NEXAFS microspectroscopy, *Environ. Sci. Technol.*, 39, 9094-9100, 2005.
- Senn, A.C., Kaegi, R., Hug, S.J., Hering, J.G., Mangold, S., and Voegelin, A.: Composition and structure of Fe(III)-precipitates formed by Fe(II) oxidation in water at near-neutral pH: Interdependent effects of phosphate, silicate and Ca, *Geochim. Cosmochim. Acta*, 162, 220-246,

2015.

- Solomon, D., Lehmann, J., Harden, J., Wang, J., Kinyangi, J., Heymann, K., Karunakaran, C., Lu, Y.,
540 Wirick, S., and Jacobsen, C.: Micro-and nano-environments of carbon sequestration: Multi-element
STXM-NEXAFS spectromicroscopy assessment of microbial carbon and mineral associations,
Chem. Geol., 329, 53-73, 2012.
- Torn, M.S., Trumbore, S.E., Chadwick, O.A., Vitousek, P.M., and Hendricks, D.M.: Mineral control of
soil organic carbon storage and turnover, *Nature*, 389, 170-173, 1997.
- 545 Xiao, J., Wen, Y.L., Li, H., Hao, J.L., Shen, Q.R., Ran, W., Mei, X.L., He, X.H., Yu, G.H.: In situ
visualisation and characterisation of the capacity of highly reactive minerals to preserve soil organic
matter (SOM) in colloids at submicron scale, *Chemosphere*, 138, 225-232, 2015.
- Vogel, C., Mueller, C.W., Hoschen, C., Buegger, F., Heister, K., Schulz, S., Schlöter, M., and
Kögel-Knabner, I.: Submicron structures provide preferential spots for carbon and nitrogen
550 sequestration in soils, *Nat. Commun.*, 5, 2947, 2014.
- Wen, Y.L., Li, H., Xiao, J., Wang, C., Shen, Q.R., Ran, W., He, X.H., Zhou, Q.S., and Yu, G.H.:
Insights into complexation of dissolved organic matter and Al(III) and nanominerals formation in
soils under contrasting fertilizations using two-dimensional correlation spectroscopy and high
resolution-transmission electron microscopy techniques, *Chemosphere*, 111, 441-449, 2014a.
- 555 Wen, Y.L., Xiao, J., Li, H., Shen, Q.R., Ran, W., Zhou, Q.S., Yu, G.H., and He, X.H. Long-term
fertilization practices alter aluminum fractions and coordinate state in soil colloids, *Soil Sci. Soc.
Am. J.*, 78, 2083-2089, 2014b.

- Wild, B., Schnecker, J., Alves, R.J.E., Barsukov, P., Bárta, J., Čapek, P., Gentsch, N., Gittel, A., Guggenberger, G., Lashchinskiy, N., Mikutta, R., Rusalimova, O., Šantrůčková, H., Shibistova, O.,
560 Urich, T., Watzka, M., Zrazhevskaya, G., and Richter, A.: Input of easily available organic C and N stimulates microbial decomposition of soil organic matter in arctic permafrost soil, *Soil Biol. Biochem.*, 75, 143-151, 2014.
- Wu, J., Wu, M.J., Li, C.P., Yu, G.H.: Long-term fertilization modifies the structures of soil fulvic acids and their binding capability with Al, *PloS one*, 9, e105567, 2014.
- 565 [Xu, R.K., Hu, Y.F., Dynes, J.J., Zhao, A.Z., Blyth, R.I.R., Kozak, L.M., and Huang, P.M.: Coordination nature of aluminum \(oxy\)hydroxides formed under the influence of low molecular weight organic acids and a soil humic acid studied by X-ray absorption spectroscopy, *Geochim. Cosmochim. Acta*, 74, 6422–6435, 2010.](#)
- Yaron-Marcovich, D., Chen, Y., Nir, S., and Prost, R.: High resolution electron microscopy structural
570 studies of organo-clay nanocomposites, *Environ. Sci. Technol.*, 39, 1231-1238, 2005.
- Yu, G.H., Wu, M.J., Wei, G.R., Luo, Y.H., Ran, W., Wang, B.R., Zhang, J.C., and Shen, Q.R.: Binding of organic ligands with Al(III) in dissolved organic matter from soil: implications for soil organic carbon storage, *Environ. Sci. Technol.*, 46, 6102-6109, 2012.
- 575 [Zhao, X., Zhang R., Xue J. F., Pu C., Zhang X.Q., Liu S. L., Chen F., Lal R., and Zhang H. L.: Chapter One-Management-Induced Changes to Soil Organic Carbon in China: A Meta-analysis, *Adv. Agron.*, 134, 1-50, 2015.](#)
- Zhu, T., Lu, X., Liu, H., Li, J., Zhu, X., Lu, J., and Wang, R.: Quantitative X-ray photoelectron

spectroscopy-based depth profiling of bioleached arsenopyrite surface by *Acidithiobacillus ferrooxidans*, *Geochim. Cosmochim. Acta*, 127, 120-139, 2014.

Figure Captions

Fig. 1. High-resolution transmission electron microscopy (HRTEM) images of highly reactive minerals from colloids extracted from soil (Ferralic Cambisol) from three long-term (1990-2014) fertilization treatments. (a), TEM images; (b), HRTEM images and selected area electron diffraction (SAED) patterns of the two regions indicated by the blue squares, showing that the black region is a complete crystalline, while the grey region is amorphous; (c-d) energy dispersive X-ray analysis (EDX) images of the region 1 and region 2. Control, no fertilization; NPK, chemical nitrogen, phosphorus and potassium fertilization; NPKM, chemical NPK plus swine manure fertilization.

Fig. 2. Representative NanoSIMS images of $^{12}\text{C}^-$, $^{27}\text{Al}^{16}\text{O}^-$ and $^{56}\text{Fe}^{16}\text{O}^-$ in soil colloids from three contrasting long-term (1990-2014) fertilization treatments (Control, no fertilization, $28 \times 28 \mu\text{m}^2$; NPK, chemical nitrogen, phosphorus and potassium fertilization, $30 \times 30 \mu\text{m}^2$; NPKM, chemical NPK plus swine manure fertilization, $25 \times 25 \mu\text{m}^2$). Note that the color intensity calibration bar displayed in the chemical maps corresponds to the relative concentrations of individual elements, but cannot be used to compare one element with another. Bar = $5 \mu\text{m}$.

Fig. 3. Box plots of $^{12}\text{C}^-/^{27}\text{Al}^{16}\text{O}^-$ (a, b) and $^{12}\text{C}^-/^{56}\text{Fe}^{16}\text{O}^-$ (c, d) ratios reflecting the $^{12}\text{C}^-$ rich ROIs (a, c) and $^{12}\text{C}^-$ less rich ROIs (b, d) of the soil colloids from three contrasting long-term (1990-2014) fertilization treatments using NanoSIMS (for all spots). Control, no fertilization; NPK, chemical nitrogen, phosphorus and potassium fertilization; NPKM, chemical NPK plus swine manure fertilization. The $^{12}\text{C}^-$ rich ROIs include the areas above 90 pixels and the $^{12}\text{C}^-$ less rich ROIs include the areas in the range of 90-40 pixels under Control and NPK, which were above 50 pixels and in the range of 50-30

pixels under NPKM. The number n in figures represents the number of the selected ROIs. The line in the middle of the box is the median value and the square in the box is the mean value. The lines that protrude out of the boxes represent the 25th and 75th population percentiles. Outliers are shown as diamonds.

605 **Fig. 4.** XPS peak-fitting (Al $2p_{3/2}$, C $1s$) images recorded from soil (Ferralic Cambisol) colloids extracted under three long-term (1990-2014) fertilization treatments. Control, no fertilization; NPK, chemical nitrogen, phosphorus and potassium fertilization; NPKM, chemical NPK plus swine manure fertilization.

610 **Fig. 5.** Fe K-edge XANES spectra of reference materials and soil colloids from three contrasting long-term (1990-2014) fertilization treatments. The scattered circles represent the linear combination fitting (LCF) results of the sample spectra. Control, no fertilization; NPK, chemical nitrogen, phosphorus and potassium fertilization; NPKM, chemical NPK plus swine manure fertilization.

615 **Fig. 6.** Fe K-edge EXAFS (left) and Fourier transforms (right) of reference materials and soil colloids from three contrasting long-term (1990-2014) fertilization treatments. Control, no fertilization; NPK, chemical nitrogen, phosphorus and potassium fertilization; NPKM, chemical NPK plus swine manure fertilization.

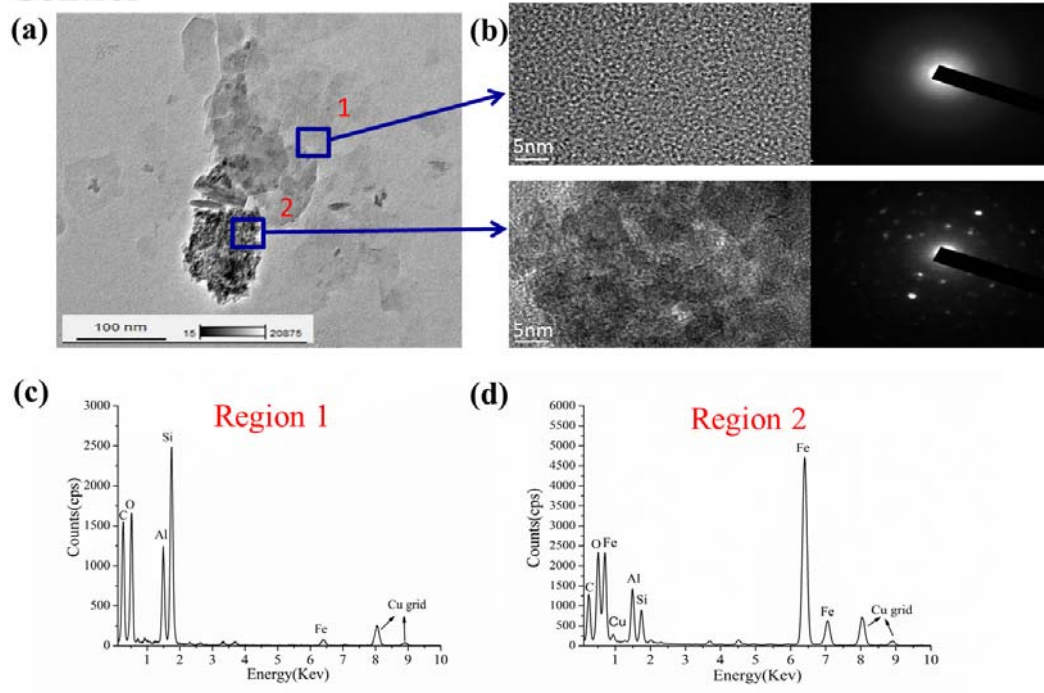
Table Captions

Table 1. Basic physiochemical characteristics of soil samples from three contrasting long-term (1990-2014) fertilization treatments ^a.

620 **Table 2.** Binding energy and quantitation/assignment of XPS spectral bands of soil samples from three contrasting long-term (1990-2014) fertilization treatments ^a.

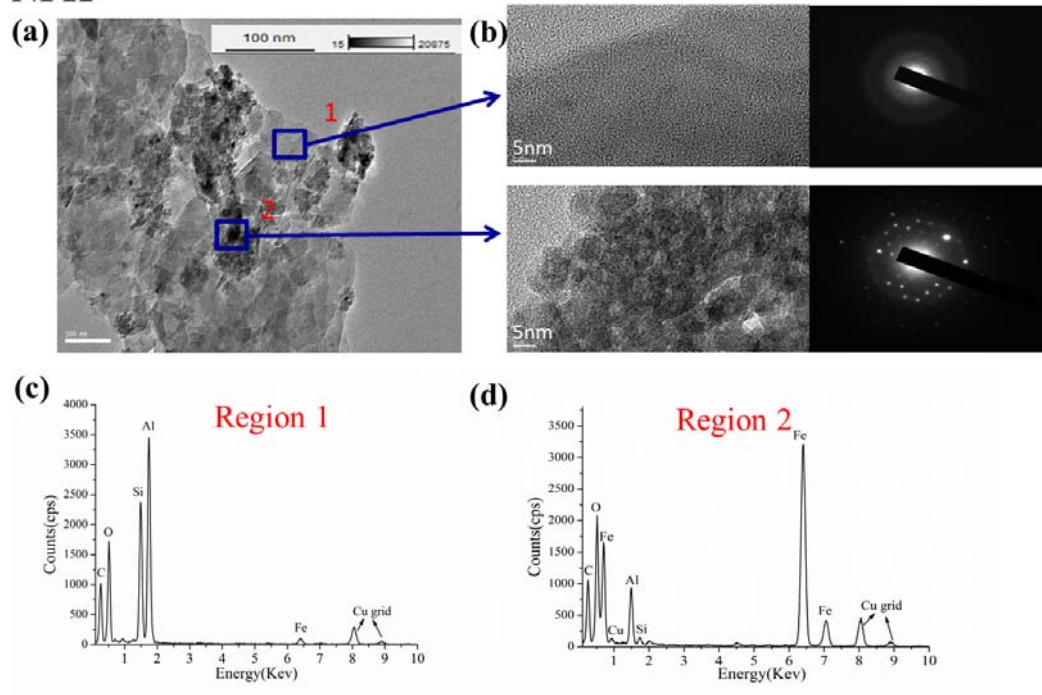
Table 3. Linear combination fit (LCF) results of Fe K-edge XANES spectra of the soil colloids from three contrasting long-term (1990-2014) fertilization treatments ^a.

Control



625

NPK



NPKM

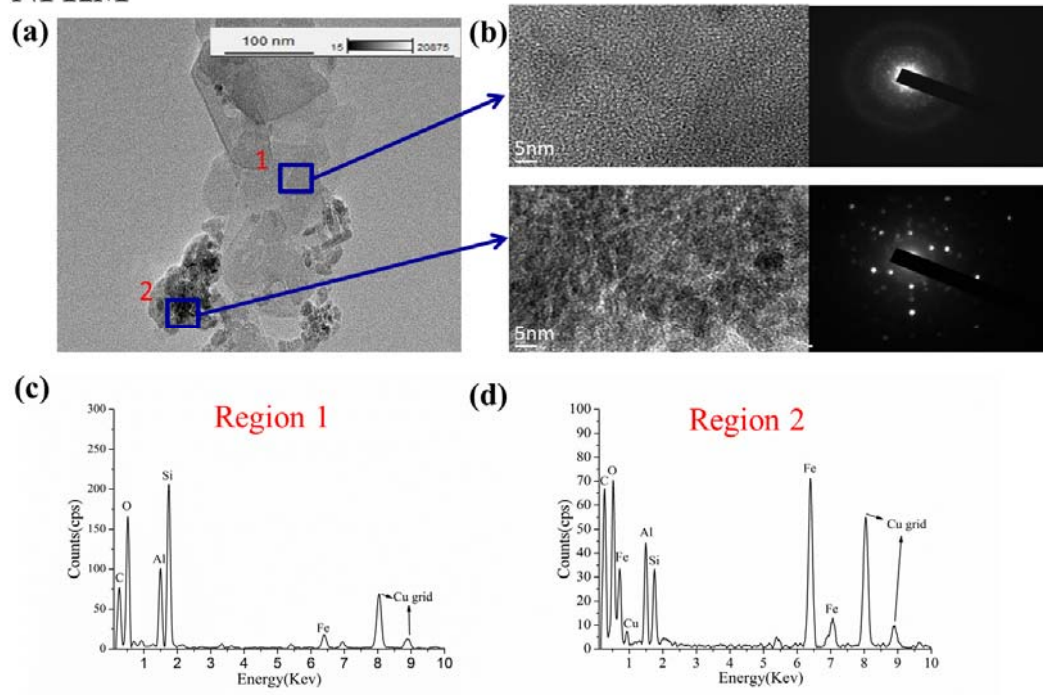
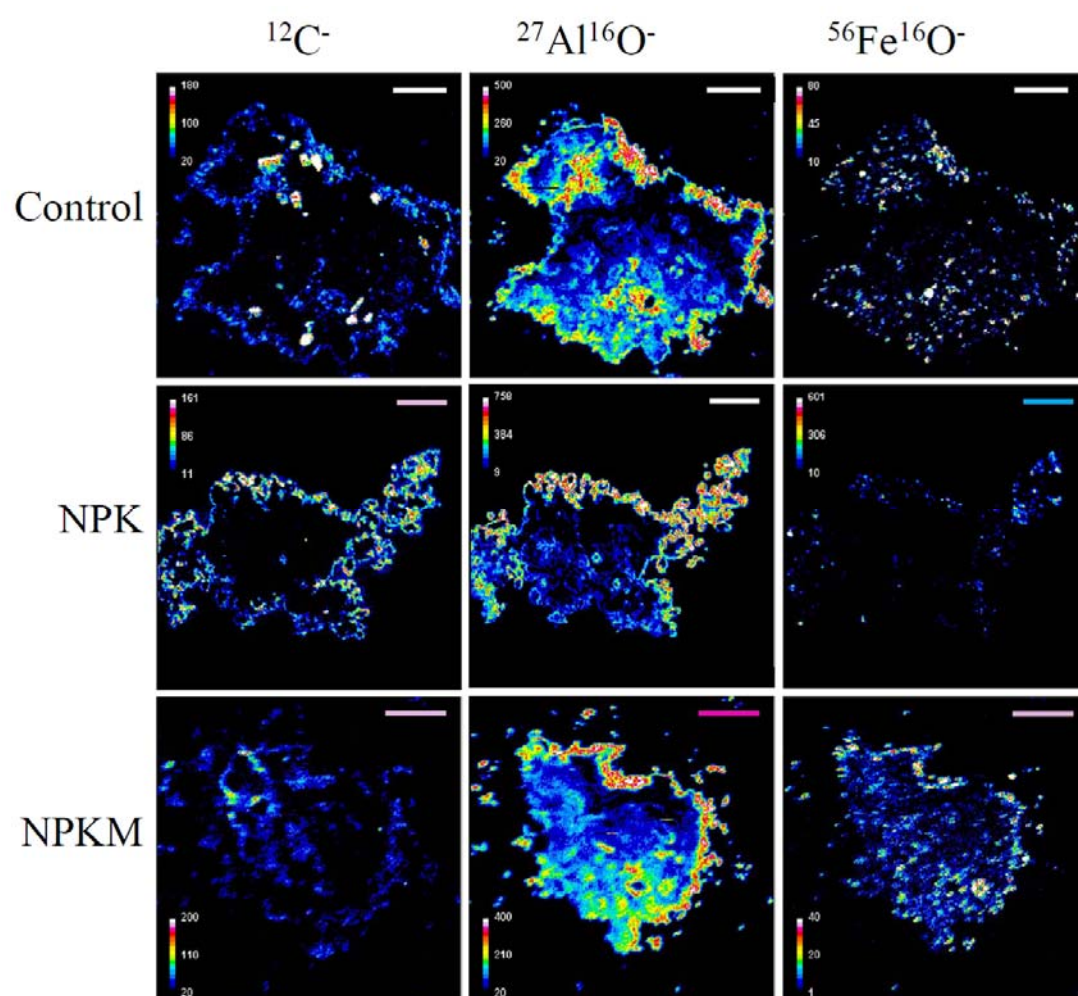


Figure 1



630 **Figure 2**

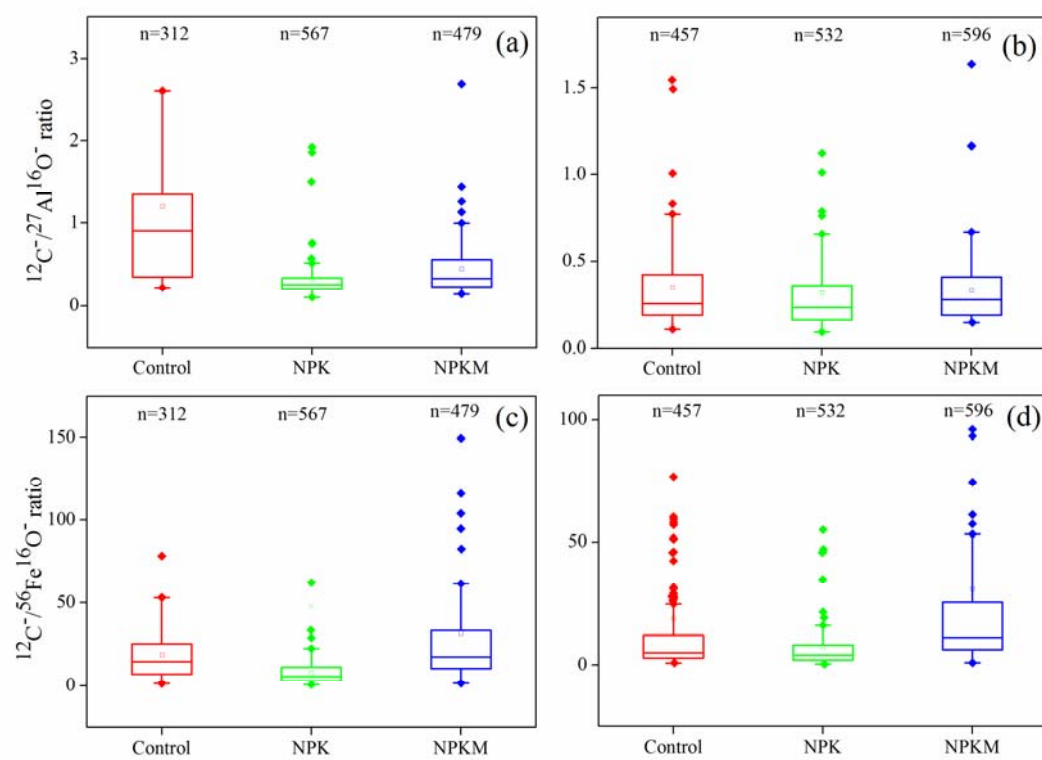
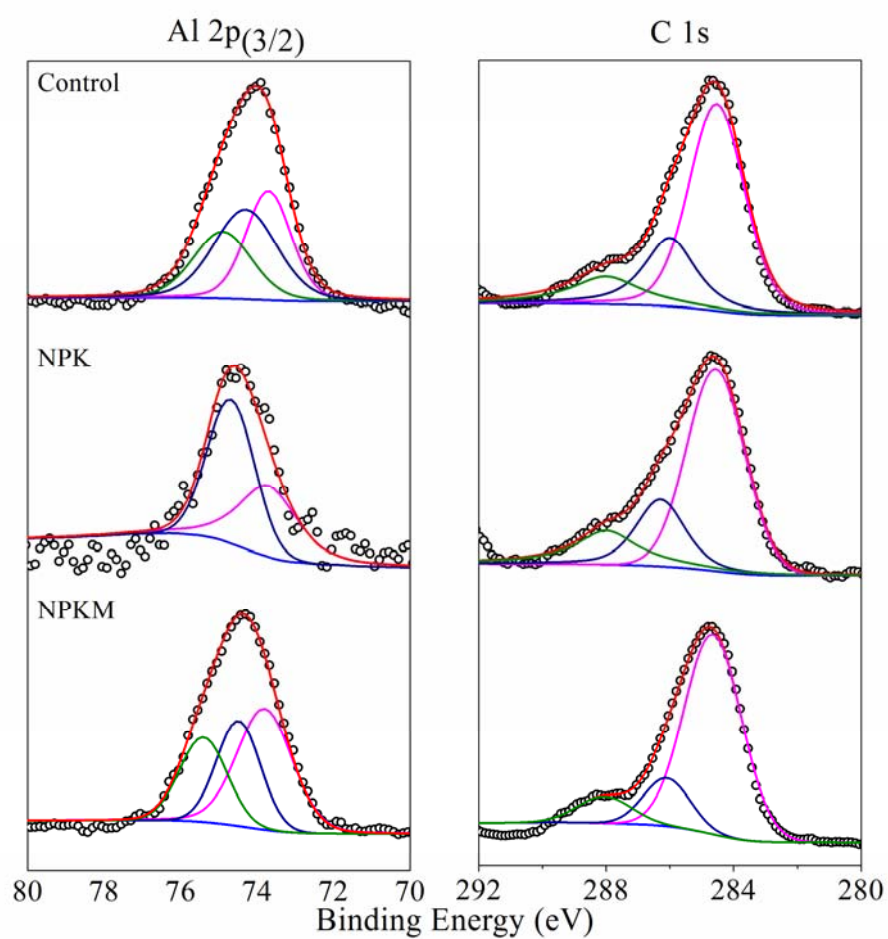


Figure 3



635

Figure 4

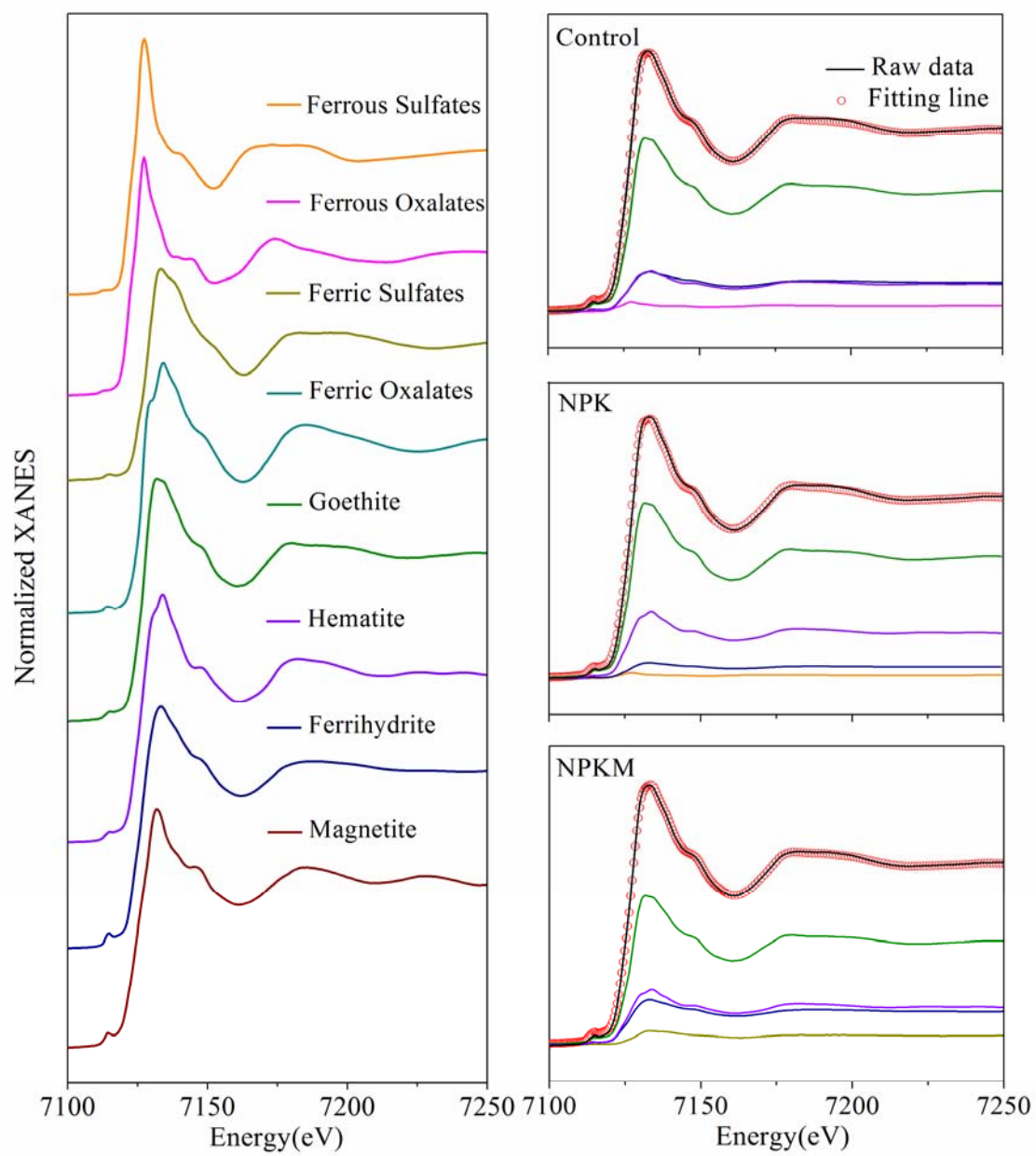


Figure 5

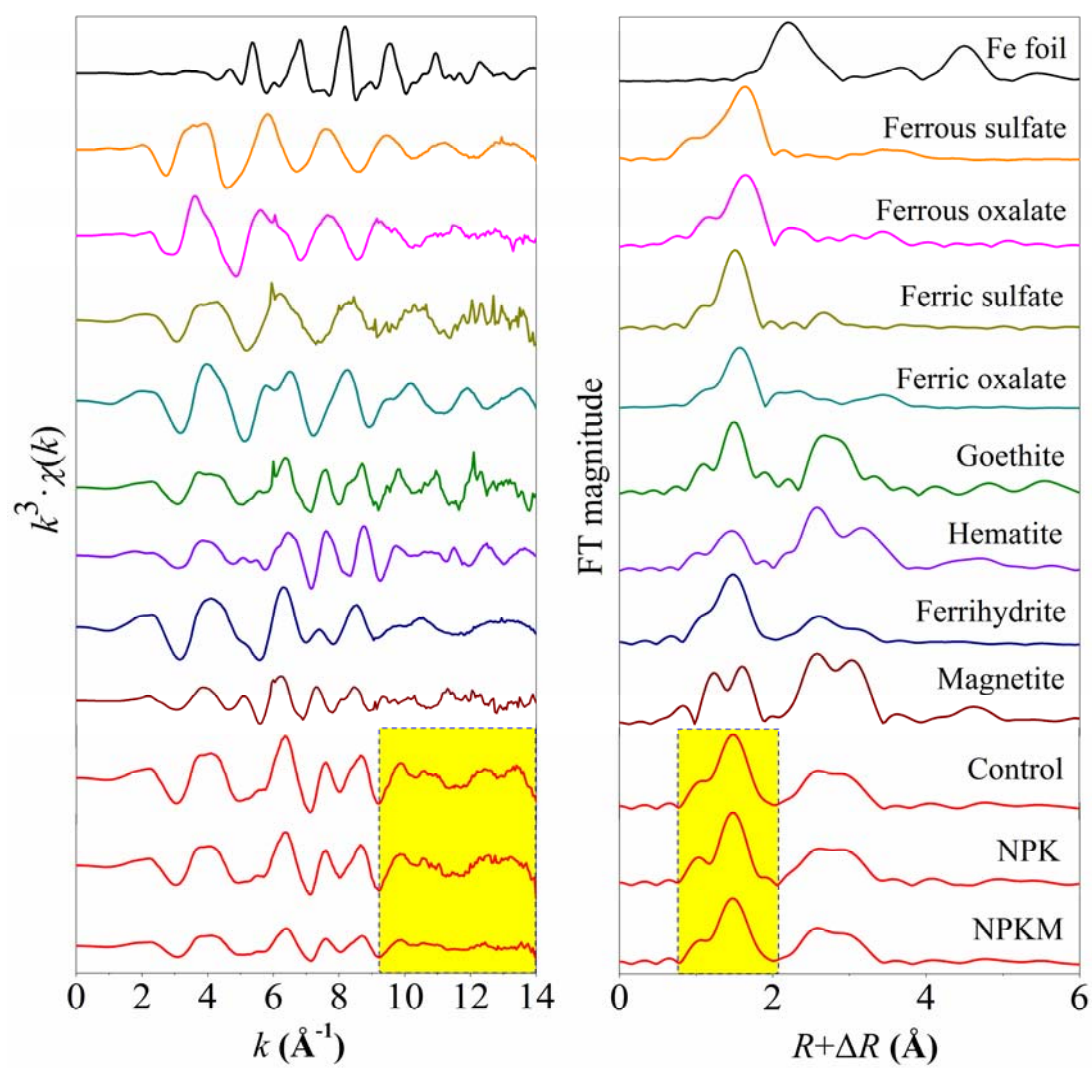


Figure 6

642 **Table 1. Basic physiochemical characteristics of soil samples from three separate long-term (1990-2014) fertilization treatments ^a.**

Treatmen	Soil					Soil colloids				
t	Bulk soil pH	SOM	Al _o	Fe _o	SRO	Al _{XPS}	Fe _{XPS}	DOC	DOC/Al _{XPS}	DOC/Fe _{XPS}
	(H ₂ O)pH	(g kg ⁻¹)	(%)	(%)	(%)	(%)	(%)	(mg L ⁻¹)		
Control	5.47 ± 0.04b	14.88 ± 2.02c	0.07 ± 0.003b	0.20 ± 0.004b	0.17 ± 0.00b	6.23	1.47	6.17	0.99	4.20
NPK	4.15 ± 0.00c	18.36 ± 0.16b	0.04 ± 0.003c	0.16 ± 0.003c	0.12 ± 0.00c	1.22	0.48	4.62	3.79	9.63
NPKM	5.84 ± 0.01a	25.13 ± 2.02a	0.11 ± 0.002a	0.30 ± 0.007a	0.26 ± 0.01a	6.84	1.59	42.02	6.14	26.43

643 ^a Note: Control, no fertilization; NPK, chemical nitrogen, phosphorus and potassium fertilization; NPKM, chemical NPK plus swine manure
644 fertilization, SOM, soil organic matter. Al_{XPS} and Fe_{XPS} indicated the surface concentration of Al and Fe in soil colloids, which were determined
645 by the X-ray photoelectron spectroscopy (XPS). Al_o and Fe_o indicated reactive Al and Fe nanominerals, which were extracted using acid
646 ammonium oxalate. DOC, dissolved organic carbon in soil colloids. Short-range ordered (SRO) minerals were calculated using the formula of
647 Al_o + 1/2 Fe_o (%) (Kramer et al., 2012). Significant differences among fertilization treatments were determined using one-way ANOVA followed
648 by the Tukey's HSD post hoc test at *P* < 0.05 after the conditions of normality and homogeneity of variance were met.

649

650 **Table 2. Binding energy and quantitation/assignment of XPS spectral bands of soil samples from three separate long-term (1990-2014)**
651 **fertilization treatments ^a.**

Element	Control			NPK			NPKM		
	Peak (eV)	Atomic (%)	Assignment	Peak (eV)	Atomic (%)	Assignment	Peak (eV)	Atomic (%)	Assignment
Al 2p_{3/2}	73.8	34.2	Allophane Al ₂ O ₃ / Al ₂ O ₃ -nH ₂ O	73.8	42.9	Allophane Al ₂ O ₃ / Al ₂ O ₃ -nH ₂ O	73.8	45.1	Allophane Al ₂ O ₃ / Al ₂ O ₃ -nH ₂ O
Al 2p_{3/2}	74.3	39.0	Boehmite AlO(OH)	74.7	57.1	Boehmite AlO(OH)	74.5	29.4	Boehmite AlO(OH)
Al 2p_{3/2}	74.9	26.8	AlOx	/	/	/	75.4	25.5	AlOx
C 1s	284.6	62.3	Aromatic carbon (Ar-C-C/Ar-C-H)	284.6	62.5	aromatic carbon (Ar-C-C/Ar-C-H)	284.6	75.9	aromatic carbon (Ar-C-C/Ar-C-H)
C 1s	286.1	23.6	Ether or alcohol carbon (C-O)	286.2	20.8	Ether or alcohol carbon (C-O)	286.1	14.7	Ether or alcohol carbon (C-O)
C 1s	288.0	14.2	Ketonic or aldehyde carbon (C=O)	288.0	16.7	Ketonic or aldehyde carbon (C=O)	288.0	9.5	Ketonic or aldehyde carbon (C=O)

652 ^a Note: Control, no fertilization; NPK, chemical nitrogen, phosphorus and potassium fertilization; NPKM, chemical NPK plus swine manure
653 fertilization. The atomic percentage (%) is the corrected value calculated from the XPS peak-fitting areas (Childs et al., 1997; Crist, 2000) and
654 elemental assignments were determined from published studies (Liang et al., 2008; Mikutta et al., 2009; Xiao et al., 2015).

655

656 **Table 3. Linear combination fit (LCF) results of Fe K-edge XANES spectra of the soil colloids from three separate long-term (1990-2014)**
657 **fertilization treatments ^a.**

Treatment	LCF results (%)						LCF parameters	
	Goethite	Hematite	Ferrihydrite	Ferric sulfates	Ferrous citrates	Ferrous sulfates	R-factor	Chi-square
Control	66.0 ± 0.025	14.9 ± 0.000	16.0 ± 0.025	ND	3.10 ± 0.012	ND	0.000052	0.00437
NPK	67.0 ± 0.025	25.0 ± 0.000	6.30 ± 0.020	ND	ND	1.70 ± 0.008	0.000051	0.00426
NPKM	56.8 ± 0.025	20.4 ± 0.000	18.0 ± 0.017	4.8 ± 0.018	ND	ND	0.000051	0.00436

658 ^a Note: Control, no fertilization; NPK, chemical nitrogen, phosphorus and potassium fertilization; NPKM, chemical NPK plus swine manure
659 fertilization. ND, not detected. Determination of parameters of fit (i.e., R-factor and chi-square) indicated that the LCF results are convincing.